CITE AS:

Audasso, E., BARELLI, Linda, BIDINI, Gianni, Bosio, B., DISCEPOLI, GABRIELE (2017). Molten Carbonate Fuel Cell performance analysis varying cathode operating conditions for carbon capture applications. JOURNAL OF POWER SOURCES, vol. 348, p. 118-129, ISSN: 0378-7753, doi: 10.1016/j.jpowsour.2017.02.081

Molten Carbonate Fuel Cell performance analysis varying cathode operating conditions for carbon capture applications

Emilio Audasso[1], Linda Barelli[2], Gianni Bidini[2], Barbara Bosio[1], Gabriele Discepoli[2,*]

[1]PERT, Department of Civil, Chemical and Environmental Engineering, University of Genova, Via Opera Pia 15, 16145 Genova, Italy

[2]Department of Engineering, University of Perugia, Via G. Duranti 67, 06125 Perugia, Italy

Abstract

The results of a systematic experimental campaign to verify the impact of real operating conditions on the performance of a complete Molten Carbonate Fuel Cell (MCFC) are presented.

In particular, the effects of ageing and ~~of different contents~~ composition of water, oxygen and carbon dioxide in the cathodic feeding stream are studied through the analysis of current-voltage curves and Electrochemical Impedance Spectroscopy (EIS).

Based on a proposed equivalent electrical circuit model and a fitting procedure, a correlation is found among specific operating parameters and single EIS coefficients. The obtained results suggest a new performance monitoring approach to be applied to MCFC for diagnostic purpose.

Particular attention is devoted to operating conditions characteristic of MCFC application as CO_2 concentrators, which, by feeding the cathode with exhaust gases, is a promising route for efficient and cheap carbon capture.

Keywords: Molten carbonate fuel cells; impedance analysis; equivalent electrical circuit; carbon capture; experimentation; cathode water effect.

* Corresponding author.
E-mail address: gabriele.discepoli@unipg.it; Tel./fax: +39 075.585.3991
Università degli Studi di Perugia, Department of Engineering, Via Duranti 67, 06125 Perugia, Italy

Nomenclature

ASR	Area Specific Resistance
CCS	Carbon Capture and Storage
CCU	Carbon Capture and Utilisation
CPE	Constant Phase Element
D	Diffusion coefficient
DRT	Distributed Relaxation Times
EIS	Electrochemical Impedance Spectroscopy
IV	Current Density-Voltage curve
L	Effective diffusion thickness
MCFC	Molten Carbonate Fuel Cell
OCV	Open Circuit Voltage
p	Pressure
P_k	Partial pressure of the species κ
P_i	i= 1, …, 8; empirical coefficients for the kinetic model
Ri	I= 1, 2, 3; empirical coefficients for resistances of the equivalent circuit
R_{TOT}	Overall cell resistance, Ω·cm^2
R_W	Resistive component of the Warburg impedance
T	Temperature, K
W	Warburg Element
WGS	Water Gas Shift reaction
y_k	Molar fraction of species κ
Z_{Im}	Imaginary part of impedance
Z_{Re}	Real part of impedance
Z_W	Generalized finite-length Warburg impedance
ΔP_{max}	Variation of the maximum power produced
ϑ	Fraction of the water vapour fed at the cathode side in the bulk that reacts with CO_2
Ψ	Diffusion Thickness
Φ	Free coefficient for the generalized finite-length Warburg impedance

1. Introduction

In the last few years, the growing concerns about global warming have strongly encouraged innovative carbon capture solutions to decrease CO_2 emissions. Several studies have shown how critical topics, such as the increasing energy demand and the related issues concerning environmental sustainability and energy efficiency, could find an answer with promising solutions. The application of Molten Carbonate Fuel Cell (MCFC) technology [1]–[4] to Carbon Capture and Storage (CCS) or Carbon Capture and Utilisation (CCU) represents one of these.

MCFCs are one of the most efficient power generators for direct energy conversion, characterized by wide operating flexibility. In addition, this technology can be exploited as CO_2 concentrator thanks to its intrinsic operating mechanism. In fact, the electrochemical reactions that take place within the MCFC involve the migration of the CO_2 from the cathode inlet to the anode outlet. During this process, the MCFC can work as power generator and, simultaneously, as CO_2 separator from an exhaust gaseous stream which can be fed to the cathode.

See Barelli et al. [5] for a detailed description of a simplified scheme of the MCFC operation as CO_2 concentrators, when installed downstream a thermoelectric plant or a combustion device included in a different industrial process. Further descriptions of similar system are described, for example, in Campanari et al. [6] or Caprile et al. [7].

This MCFC configuration was investigated in several previous works, involving both experimental [8]–[11] and modelling [6], [12]–[21] activities as well as correlated topics as the fuel/oxidant pollution problems [19], [22]–[24] and the material performance optimization [25], [26].

MCFCs are flexible from the point of view of the fuel which can be used [27], but also allows the use of a wide range of mixture compositions as oxidant.

The basic conditions required for the cathodic feeding are a CO_2 concentration above 5% and a partial

pressure ratio P_{O_2}/P_{CO_2} higher than 0.5 for low O_2 content (< 4-5%) [10].

Usually these constraints can be respected in CCS or CCU applications and MCFC can be used to concentrate CO_2 from various sources: from power production (e.g. based on reciprocating internal combustion engines, combined cycles or coal plants [28]) to industrial processes (21% of 2013 greenhouse gas emissions associated with human activities in U.S. can be ascribed mainly to cement, iron and steel production [29]).

~~Nevertheless, similar applications can involve operating conditions near to critical working points, for example due to a low CO_2 content, so that the monitoring of performance and degradation results particularly important.~~ Nevertheless, similar applications can involve MCFC working close to the bounds of its operating domain, for example when the treated exhaust gas has a low CO_2 content. In these cases, it is fundamental to monitor the MCFC performance and degradation. In addition, the effect of the presence of water at the cathode side, expected in CCS, CCU and in general other industrial applications, is another topic to be deeply investigated.

In this scenario, Electrochemical Impedance Spectroscopy (EIS) is proposed as a powerful tool to assess the MCFC performance. EIS analysis allows the isolation effects of the electrochemical reactions occurring in the cell and allows the identification of the corresponding basic operating parameters, following the pioneering works of Selman *et al.* [30] or Nishina *et al.* [31]. This technique is under continuous development and improvement, for example the novel approach to the EIS interpretation through the distributed relaxation times (DRT) method is very promising [32], [33].

In literature, many works exploit EIS interpretation for in-depth electrochemical analysis. These works are usually limited to materials characterization [34], [35] by operating on simplified fuel cell systems (i.e. button cell or half-cell), in safe or particular (to point out specific aspects) conditions [36], far from the realistic operative ones.

Rough assessments of MCFC performances, operated specifically in CCS or CCU configuration and in

real working conditions, were performed by several authors [11], [37]–[39]. Nevertheless, a systematic discussion is not conducted and the experimental results are not analytically correlated to the imposed operating conditions.

The main aim of the present study is to analyse the correlation between the EIS data and the variation of relevant operating parameters on a complete MCFC tested in real working conditions characteristic of a CCS or CCU configuration. In addition, particular attention is devoted to the effect of the water presence at the cathode side.

Each investigated operating point, defined by a specific cathodic mixture and ageing, is characterized through current density-voltage (IV) curve and EIS analysis.

To provide a systematic mapping of the MCFC performance, the cathodic mixture is varied by modifying the relative content (in terms of molar fraction) of the O_2, CO_2, and H_2O species, keeping constant the overall flow by balancing with nitrogen, as inert inside the cell. As a result, the IV and the EIS parameters inferred from the experimental campaign are fully characterized enabling their proper correlation to the variation of a specific operating parameter. The obtained IV curves and EIS spectra are presented and discussed in the present paper.

These results, based on the experimental evidence of a complete cell, have an impact opening routes to monitor the MCFCs performances for diagnostic purpose. Indeed, EIS is a well attested method as diagnostic tool in the fuel cells dedicated literature [40], [41], mainly for solid oxide fuel cells (e.g. [42]–[44])~~, but also in the~~ and MCFC field [36], [45], [46]. The present work adopts this philosophy, usually applied to fuel cell degradation monitoring, and extends it to the monitoring of the fuel cell performance due to the change of working points (i.e. the particular cathodic mixture), distinguishing the impedance spectrum variations due to degradation and operating conditions.

In particular, an equivalent electrical circuit is proposed and the dependence of its main components on the operating conditions is highlighted, suggesting an empirical correlation from these results and the

main phenomena affecting MCFC performance.

The work, related to a reference behaviour and its deviation, constitutes a basis for future investigations for developing a dedicated diagnostic tool.

2. Experimental

2.1. MCFC operating principle

Conventional MCFCs exploit Ni-based catalyst (electrodes) to support the following electrochemical reactions (1-(3) and produce current:

$$\frac{1}{2}O_2 + CO_2 + 2e^- \rightarrow CO_3^= \qquad \textit{(cathode)} \qquad (1)$$

$$H_2 + CO_3^= \rightarrow H_2O + CO_2 + 2e^- \qquad \textit{(anode)} \qquad (2)$$

$$H_2 + \frac{1}{2}O_2 + CO_2^{cathode} \rightarrow H_2O + CO_2^{anode} \qquad \textit{(total)} \qquad (3)$$

~~Together with the previous ones, also the~~ Along with the above reaction, Water Gas Shift reaction (WGS) is to be taken into account because it highly affects the anodic exhaust composition since it quickly reaches the equilibrium in the analysed condition [47]:

$$CO + H_2O \leftrightarrow CO_2 + H_2 \qquad \textit{(water gas shift)} \qquad (4)$$

The cathodic reaction (1) produces the ion $CO_3^=$ that, moving throughout the molten carbonate electrolyte, closes the electrical balance at the anode side, via reaction (2) [48], given eq. (3) as the global reaction. This implies that the MCFC needs a source of CO_2 to work efficiently. At first glance, ~~it seems~~ it is observed as a limiting condition. Actually, it represents the key feature that allows the carbon separation from a general mixture (e.g. an exhaust off-gas) containing CO_2. It is driven from the cathode to the anode, where it is concentrated in a mixture composed by CO_2, water and unreacted fuels, mainly hydrogen. Thereafter, the CO_2 contained in the anodic off-gases can be separated through further oxidation of the unreacted fuel and subsequent water condensation. It should be remarked that in MCFCs the CO_2 is not produced, but is just a vector to carry the electric charge on the oxide ion via a carbonate

ion throughout the electrolyte, from cathode to anode.

In addition, it is worth to be noted that the presence of water at the cathode side, typical of CCS, CCU as well as other industrial applications, promotes the following chemical reaction:

$$O^{=} + H_2O \leftrightarrow 2OH^{-} \quad (5)$$

This reaction, involving the oxygen ions which can be present as intermediate reactants of (1), provides an alternative reaction path to the conventional reaction (1) for the $CO_3^{=}$ formation:

$$2OH^{-} + CO_2 \leftrightarrow CO_3^{=} + H_2O \quad (6)$$

This aspect has been deeply discussed by the authors in the parallel modelling work [49] and is object of experimental validation in the following sections of the present paper.

2.2. **Set-up and methodology**

The performance of a single MCFC fed with a gas mixture simulating the exhaust gas composition of a combined cycle power plant characterized by a 6% of CO_2 is evaluated.

The tested MCFC, supplied by FCES (*FuelCell Energie Solutions GmbH*), has a planar square area of 79.21 cm^2 (8.9x8.9 cm). The anode consists of a Ni structure, the cathode is constituted by a NiO-based material and the electrolyte is composed by a mixture of lithium and potassium carbonate (details are not available because of confidentiality). The fuel cell is a sort of sandwich composed by, starting from the inside, an electrolyte (included in an alumina based inert matrix), two electrodes, two current collectors and stainless steel frames which supply the gas, expel the exhaust gases and drain the collected electric current. The MCFC is tightened by a mechanic load of 2.2 bar produced by a hydraulic piston to avoid gas leakage across the cell boundary. The test facility layout is already described in ~~details~~ detail in [48]. The main used instruments are Brooks 5850E Digital Mass Flow Controllers (±0.7% of rate and ±0.2% F.S.), Agilent Technologies DC Electronic Loads N3304A (current resolution: 0.1 mA; current accuracy: ±0.05% + 5 mA; voltage resolution: 0.1 mV; voltage accuracy: ±0.05%+ 3 mV) and 33220A Function/Arbitrary Waveform Generator (frequency range: 1 μHz – 20 MHz).

A homemade software installed in a remote computer manages all the equipment. The test bench operates in current mode. Each point of the IV curve is measured by measuring the voltage at 1 Hz of frequency for at least 10 minutes after the fuel cell is stabilized. The final value for each parameter is obtained by averaging all the collected data during this stable phase.

Each operating condition is characterized by a standard IV polarization curve and by EIS analysis.

It is remarked that the EIS curves are collected under current density load in the range 25 - 40 $mA \cdot cm^{-2}$, to better characterize the MCFC under real operating conditions. It is well known, indeed, that the fuel cell impedance spectrum significantly changes with the electric load [37], [41], [50]–[52]. Consequently, measurements are carried out under load by applying different current values, avoiding operation at OCV. The corresponding fuel utilization factor range is within the range 12-18%, while at the cathode the O_2 and CO_2 utilization factor ranges are, respectively, 3-13% and 14-23%, due to the applied current and cathodic feeding variations (see section 2.3). Nevertheless, this choice implies a slight loss in the measurement precision at low frequencies. Below 1 Hz, in fact, the increase in noise related to higher values of current can be critical.

2.3. Test campaign

The test campaign is organized to characterize the impact of ageing and cathodic mixture on the MCFC impedance elements. The cathodic reference composition (shown in Table 1) is chosen to reproduce a realistic generic exhaust off-gas of interest for carbon capture purposes, while the anodic one is a standard laboratory composition [20], [23] (80% H_2 20% CO_2, on dry basis). The latter is kept constant for the whole test campaign to obtain a low and constant anodic polarization, avoiding severe anodic operating conditions (i.e. high fuel utilization factor) and isolating only the cathode effects on the fuel cell behaviour.

The total flow rates, kept constant to avoid fluid-dynamic effects on the mass transport and consequently on the polarisation contribution, are 11.5 $Nl \cdot h^{-1}$ at the anode and 110.3 $Nl \cdot h^{-1}$ at the cathode. A working

temperature of 650°C completes the operative framework definition.

Table 1. Reference feeding compositions expressed on a volumetric basis.

Gas type	Reference Anode Composition	Reference Cathode Composition
CO_2	16%	6%
H_2	64%	-
H_2O	20%	9%
N_2	-	73%
O_2	-	12%

Starting from this reference operating condition, each single parameter is varied by keeping all the others constant. Specifically, the cathodic species contents are varied according to the values summarized in Table 2. Each tested condition is characterized through IV curve acquisition and EIS analysis.

The CO_2 fraction range of 4%-17.5% is chosen to match important case studies when the MCFC operates as CO_2 concentrators, installed downstream a thermoelectric plant or a combustion device included in a different industrial process. Just as example, a natural gas combined cycle power plant produces an exhaust stream with about 4% of CO_2 [53] , while a natural gas reciprocating engine produces an exhaust gas with about 8% of CO_2 [10] and a coal fired power plant produces an exhaust stream with above 12% of CO_2 [28]. A cement plant has also higher concentrated CO_2 emission, depending from the sampling point on the production process [16], [54].

At the cathode, in particular, the mutual dependence between carbon dioxide and water contents is investigated by testing, for each H_2O content value, all the chosen CO_2 compositions, maintaining the reference O_2 content and temperature. For the O_2 content variation, instead, the values indicated in Table 2 are tested, with all the other parameters fixed at their reference values. As mentioned above, the overall cathodic flow rate is maintained constant, by balancing with N_2, to isolate the effects of the composition, avoiding the influence of fluid dynamics on diffusion transport phenomena.

Table 2. Parameters variation considered for the definition of the test campaign (composition expressed on a volumetric basis).

Cathode gas type	**Tested Compositions**		
CO_2	4%	6%	17.5%
H_2O	0%	9%	20%
O_2	5%	8%	12%

Finally, performance characterization (acquisition of IV curves and EIS spectra) under the reference condition is repeated three times during the overall test campaign and, more specifically, at the tests beginning (0 h), after 327 hours and at the end (after 629 hours) of the campaign to characterize ageing effects on MCFC performance.

2.4. Results

The IV curves and EIS spectra dependence on the single gas content at the cathode are firstly discussed. IV polarization curves, and the relative power curves, are ~~visible~~ shown in Figure 1. As expected, all the IV recorded curves improve (in particular at high current densities) by increasing the fraction of CO_2 and O_2 in the cathodic mixture. These experimental results are in good agreement with [8], [10], [55], [56]. Nevertheless, it is interesting to note how the increase of the H_2O content at the cathode side also improves the performance and how this voltage gain becomes higher when the CO_2 or H_2O content is lower (Figure 1, A). Similarly, the impedance spectra present general benefit when CO_2, H_2O and O_2 contents increase, as visible in Figure 2, with particular attention to graphs A and B. Moreover, coherently with the progress of degradation phenomena, ageing negatively affects MCFC impedance (Figure 2, C).

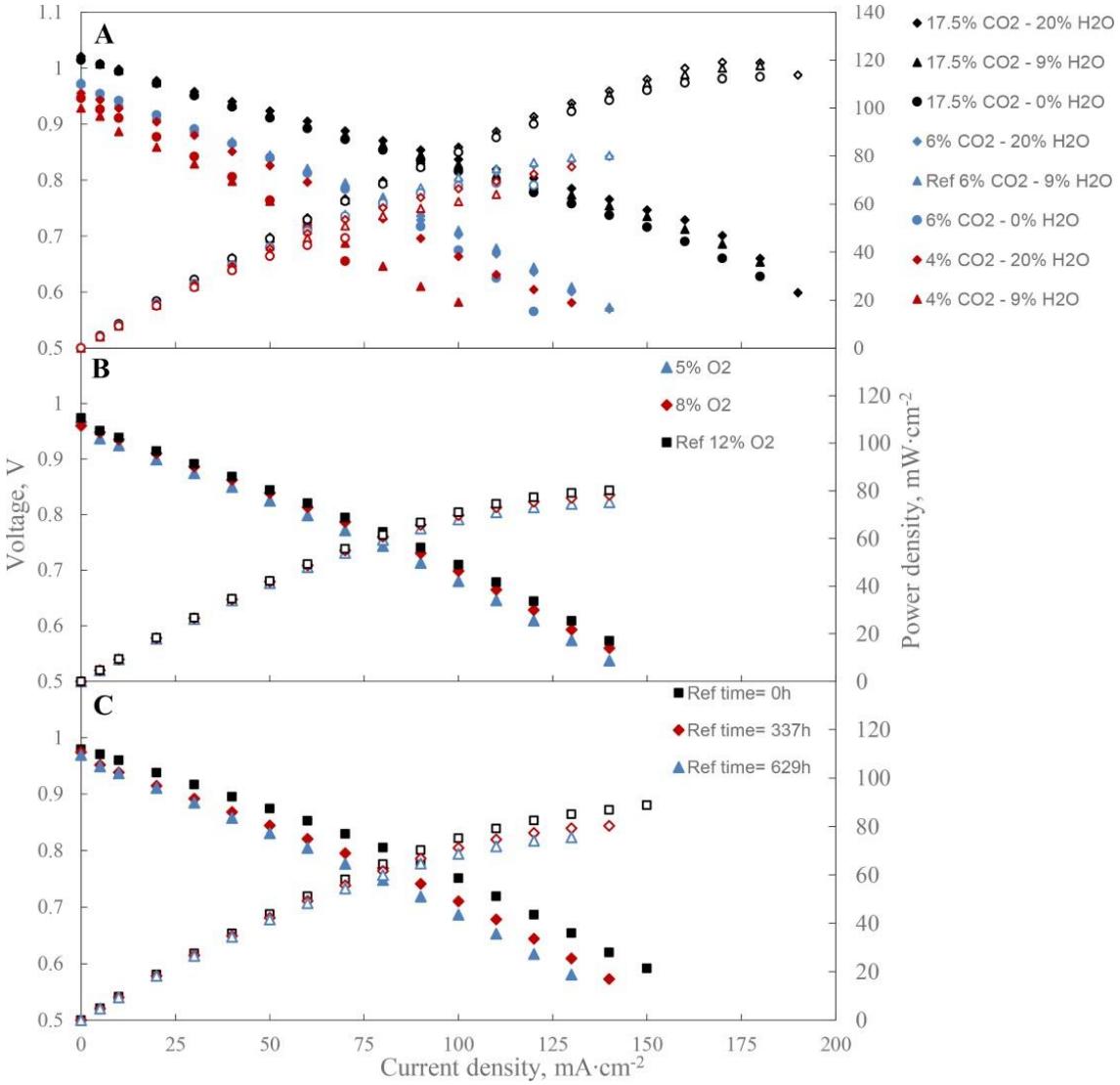

Figure 1. IV polarization curves (solid symbols) for different values of carbon dioxide and water contents (A), oxygen content (B) and ageing measurement (C). The corresponding open symbols represent the relative power curves.

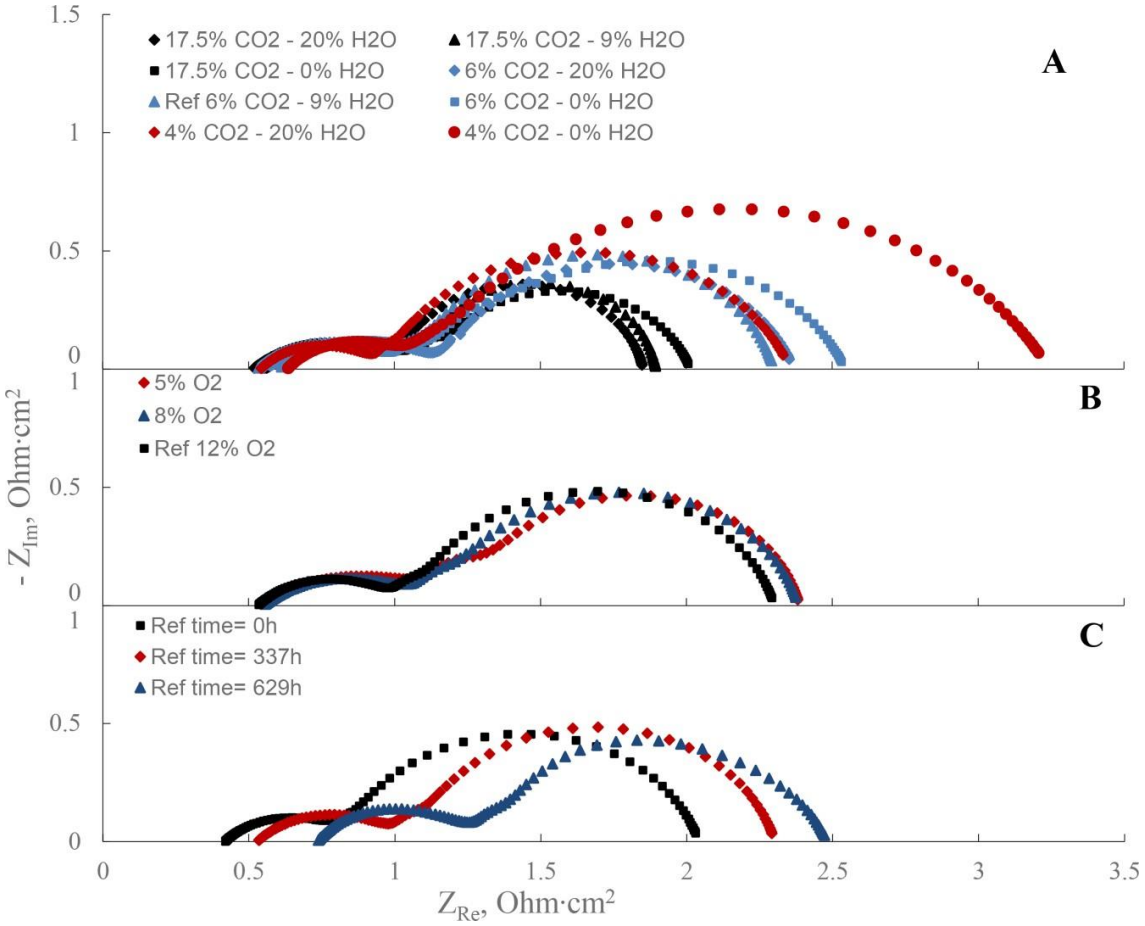

Figure 2. EIS curves for different values of carbon dioxide and water contents (A), oxygen content (B) and ageing measurement (C).

2.4.1. Effects of CO_2 variation

Figure 1, A and Figure 2, A show all the IV curves and EIS spectra recorded for different CO_2 and H_2O values at the cathode inlet, respectively. As expected, the increment of the CO_2 concentration induces an increment in the measured voltage. This effect leads to large changes in both OCV and the slope of the IV curves. The global trend of the maximum power produced by MCFC, for different levels of CO_2, reflects a similar behaviour for the different H_2O contents (see section 2.4.2). Specifically, regarding the carbon dioxide, for example under dry cathode feeding conditions, the gain in the produced maximum power with 17.5% of CO_2 is almost 150% higher with respect to the case with 4% of CO_2 (Figure 1, A). The EIS behaviour (Figure 2, A) reflects the IV trend. The curves, in fact, are gathered together according to the CO_2 content (higher impedance for lower CO_2 content). Moreover, each bundle characterized by

the same CO_2 content shows the impedance trend as a function of the H_2O percentage, putting in evidence that lower water content results in higher impedance.

2.4.2. Effects of H_2O variation

Despite cathodic water is not directly involved in the main MCFC reactions, the voltage is clearly function of it (as evident in Figure 1, A), in agreement with Sugiura et al. [8]. In particular, voltage improves for higher H_2O contents, according to the mechanism described by eqs. (5) and (6) (see section 1) as discussed e.g. by Nishina et al. [57] and Hemmes et al. [58], as well as deeply investigated by the authors in [49] referring to these same experimental results. It is clearly visible in Figure 1, A that H_2O strongly affects the IV curves slope and plays a major role for low CO_2 contents.

The maximum power produced exhibits a similar trend. For example, if 20% of H_2O is added, a maximum power gain is always obtained respect to the reference case. Anyway, such a gain varies from 60% down to few percentage values if the CO_2 content is increased from 4% up to the highest content of 17.5%.

Finally, impedance spectra exhibit a trend analogous to the one observed for the voltage, showing that the overall impedance decreases while the H_2O content increases. The in-depth EIS analysis is discussed in section 3.

2.4.3. The effects of O_2 variation

The O_2 enrichment enhances the performance (Figure 1, B) just slightly, if compared to the effects due to H_2O and CO_2: the maximum power production increases by 6% with the oxygen fraction increment from 5% to 12% (for comparison see the power curves for different H_2O and CO_2 concentrations).

The respective EIS curves show small size reductions in the overall impedances in the Nyquist plot (Figure 2, B).

Moreover, in the range of 1 – 1.5 Ohm·cm^2 of the real impedance $Z_{Re,}$ the EIS spectra shows changes as

function of the oxygen content. They can be ascribed, as discussed in the following Section 3, to a stronger impact of the Warburg coefficient at low O_2 contents.

2.4.4. Effects of ageing

During more than 650 hours of test, the MCFC showed a performance decrease of about 15% of the maximum power produced (Figure 1, C - top box) followed by a general lowering of the output voltage as evident from the IV curves. The EIS (Figure 2, C) measurements show an increase in the internal resistance, corresponding to a global shift of the ~~whole~~ all curves towards higher values of the real impedance (Z_{Re}).

3. Theoretical equivalent circuit

The EIS experimentally obtained are fitted according to the method of Lee and Selman [45], for the equivalent circuit selection.

It consists of a standard double Randles–Ershler circuits (as in Ref. [59]), where the capacities are replaced with CPEs. The CPE elements, requested by the strongly depressed semicircles (in Figure 2 the relative centre is on the lower quarter of the Nyquist plot), correspond to the distortion of the capacitance due to finite thickness and surface roughness of the electrode [60]. Recent studies set a limit on the dependence on roughness at medium and high frequencies of the CPE behaviour where the deviation from the ideal response can be explained by the non-uniform current and potential distribution along the electrode surface [61].

Regarding the three identified resistances, $R1$ is usually assessed in the Nyquist plot as the intercept of the impedance curve with the *x-axis* and is related to the internal resistance. $R2$ belongs to the first mesh which describes the first impedance arc, for frequencies in the range 1 kHz - 0.01 kHz, and $R3$ belongs to the second mesh, relative to the low frequencies impedance arc (below 0.010 kHz).

Furthermore, a Warburg element [62], which takes into account all the spectra features according to the

acquired data, is necessarily added to obtain a satisfying fit. In fact, some series – tests at different water and oxygen contents – show a third little circle between the two main semicircles in the Nyquist plot. This is an evidence of a hidden impedance component which contributes (together with $R2$) to the growth of the saddle point and depends on H_2O (Figure 2, A) and O_2 contents (Figure 2, B).

In Figure 3, A and Figure 3, B the results of the fits with and without the Warburg coefficient are compared.

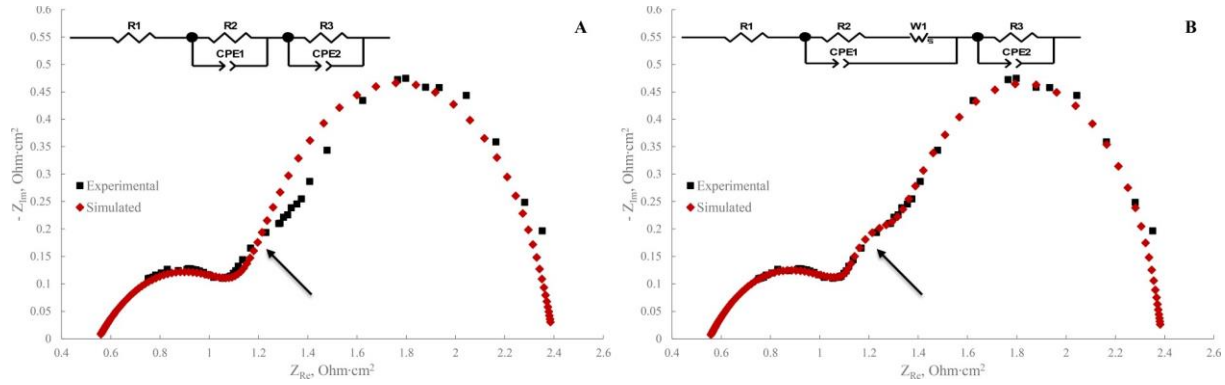

Figure 3. Fit (red) of the experimental data (black) without (A) and with (B) the Warburg element in the equivalent circuit, showed on the top of the figure. Between the two main impedance semicircles, the black arrow highlights a third small one describable through the Warburg element.

This modified Randles-Ershler circuit mesh is already used, for example, in [63]. It was validated, through suitable fitting procedures, that this model better addresses the experimental impedance behaviour, with respect to the case of simple addition of an extra circuit mesh containing another R-CPE parallel.

In general, the form of the Warburg impedance Z_W is described by equation (7).

$$Z_W = R_W \cdot \frac{\tanh(i\Psi\omega)^{\Phi}}{(i\Psi\omega)^{\Phi}} \qquad (7)$$

Where:

- R_W is the resistive component of the Warburg impedance
- Ψ is defined as L^2/D (L is the effective diffusion thickness while D is the diffusion coefficient)

- Φ is a free coefficient that generalizes the finite-length Warburg impedance [64], obtained for $\Phi = 0.5$.

An interpretation of the physical meaning of all the circuit components is proposed in the following sections.

4. Discussion

To study how the impedance spectra vary according to the main working conditions and operating parameters we focus attention on the resistances $R1$, $R2$, $R3$ and R_W.

More specifically, our goal is to determine which parameters of the equivalent circuit are more representative of the MCFC performance variation.

The CPE parameters are not taken into account because: i) as general behaviour, they do not add more information if referred to the resistances and ii) the second loop CPE parameters are ambiguous since they are strongly affected by the Warburg impedance, when it is relevant, as discussed in Section 4.4.

The analysis is carried out considering impedance spectra characterized by the middle frequencies affected only by cathodic kinetics [65], while the anodic contribution is assumed negligible. This contribution can be assumed negligible not only because generally the anodic polarisation is lower than the cathodic one, but also because the ~~very favoured~~ favourable anodic operating conditions results in a further lower anodic polarisation. In addition, these anodic conditions are kept constant throughout all the experimentation, so that they do not affect the impedance variations coming from the different tested cathodic compositions. From Figure 4 to Figure 7 the trends of the investigated parameters are shown.

4.1. Resistance parameter $R1$

$R1$ trend was determined as function of the changes in the working conditions at the cathode. The results are summarized in Figure 4.

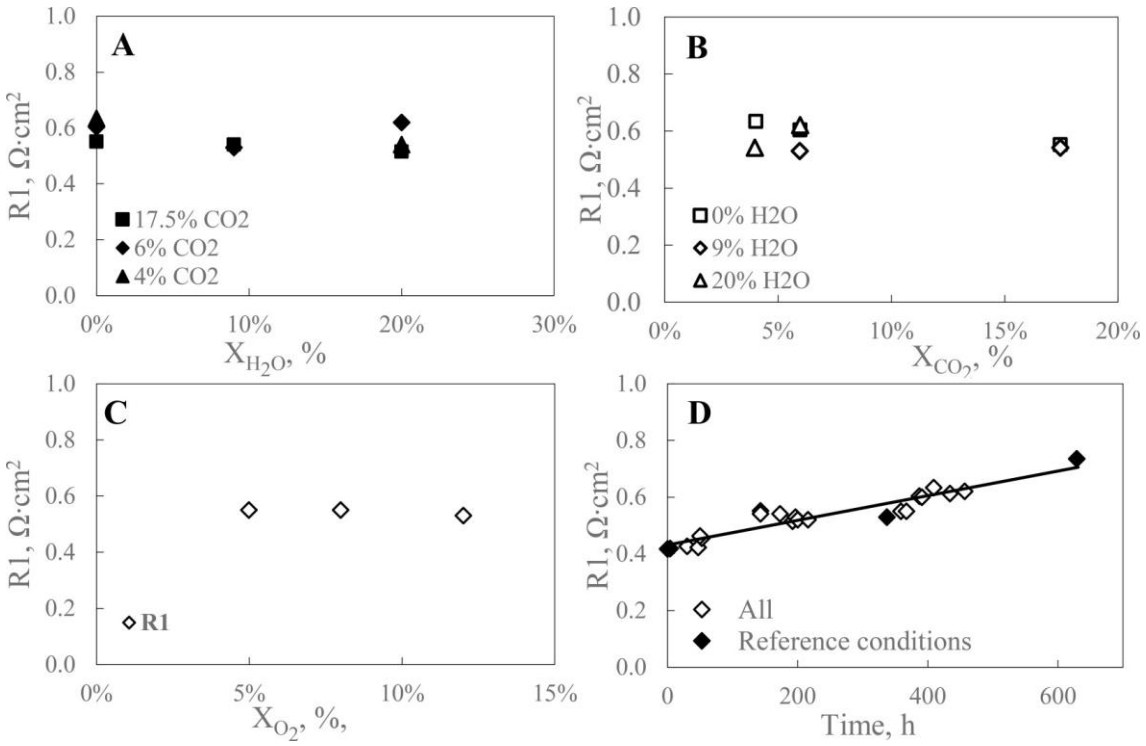

Figure 4. R1 dependence on the cathodic species content: water (A), carbon dioxide (B) and oxygen (C). R1 dependence on time (D) for the reference conditions (solid diamond) the whole test series (open diamonds).

$R1$ does not exhibit a clear and monotonic dependence on the cathodic feeding composition (Figure 4, A, B and C), while it depends on ageing as evident from the monotonic trends shown in Figure 4 (graphs D).

The performance degradation, previously observed in the IV curves (Figure 1, C), can be correlated with the increase in the internal resistance, mainly due to contact resistance, even though a minor contribution of an electrolyte loss is also possible. In particular from graph D of Figure 4 it is evident the strong correlation between $R1$ and the degradation phenomena, highlighting the relevance of $R1$ from a diagnostic point of view. Moreover, this correlation, valued on the whole test campaign, is linear (Figure 4, D); after 600 hours, $R1$ increases of about 70%, representing the predominant part of the entire variation of the EIS curve.

Such a result proposes $R1$ is a suitable parameter to be monitored for the analysis of the ageing effects.

4.2. Resistance parameter *R*2

Similarly to the *R*1 case, the main operating parameters were varied to investigate their effect on *R*2. The results are shown in Figure 5.

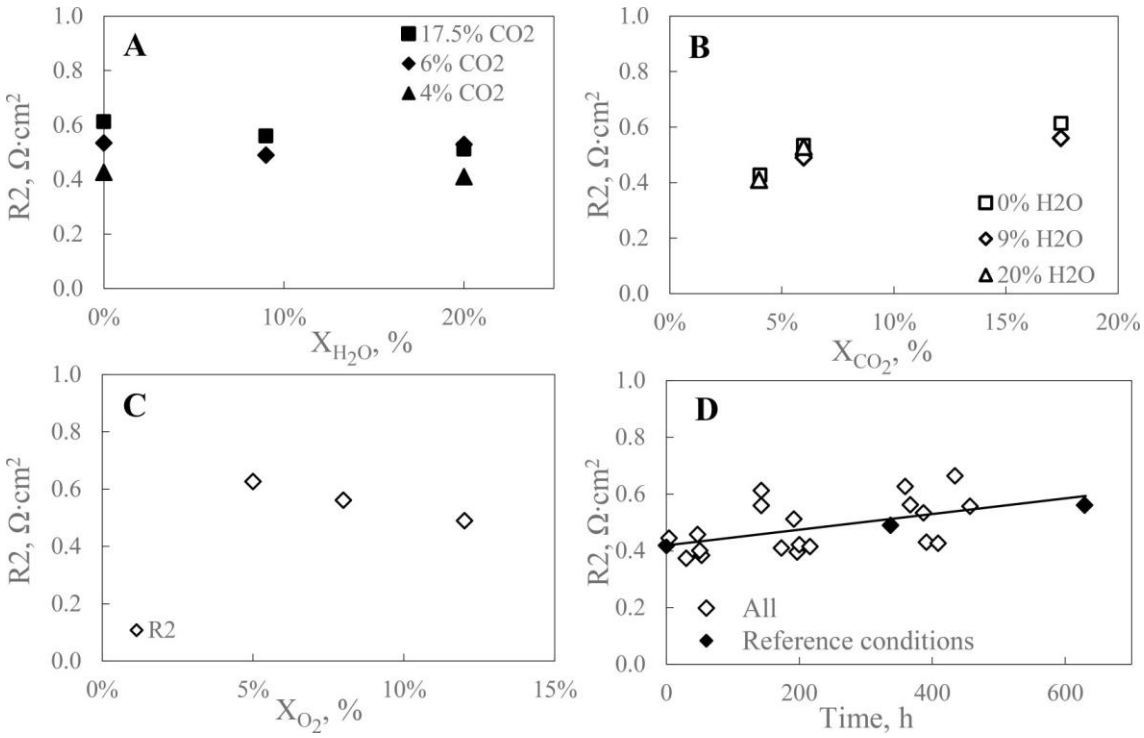

Figure 5. R2 dependence on the cathodic species content: water (A), carbon dioxide (B) and oxygen (C). R2 dependence on time (D) for the reference conditions (solid diamond) the whole test series (open diamonds).

The general trend of *R*2 can be highlighted as:

- it slightly decreases while the H_2O concentration increases (Figure 5, A), ~~more markedly~~ remarkably at high CO_2 contents;
- it decreases while O_2 concentration increases (Figure 5, C);
- it increases proportionally to the CO_2 concentration (Figure 5, B).

Such behaviour suggests that *R*2 may be correlated to the O_2 reaction mechanism. In fact, in literature, two main possible paths for the O_2 evolution are described [30], [35]: peroxide and superoxide paths. Both of them are limited by the diffusion of the oxygen ions and involve a resistance that increases when the CO_2 concentration grows or the O_2 concentration decreases [37].

The water effect is not very significant. However, ~~the presence of water can be seen as a factor that facilitates the diffusion of reactants thanks to the discussed additional reaction path offered to superoxide ions according to reaction~~ the presence of water can facilitate the diffusion of reactants. This is due to the additional reaction path for the superoxide ions according to reactions (5) and (6). Consequently, the presence of water produces a resistance reduction particularly visible in more critical conditions (in this context when CO_2 concentration is higher).

The effect of ageing on $R2$ is significantly lower with respect to effect on $R1$. In fact, during the overall test (Figure 4, D), $R2$ increases by 33%.

In conclusion, the obtained results suggest that $R2$ is the most suitable parameter to be monitored for the analysis of the effects of O_2 on the MCFC performances, while ageing effects are well described by the trend of parameter $R1$, as already discussed above.

4.3. Resistance parameter $R3$

In the following Figure 6, the results for $R3$ are reported.

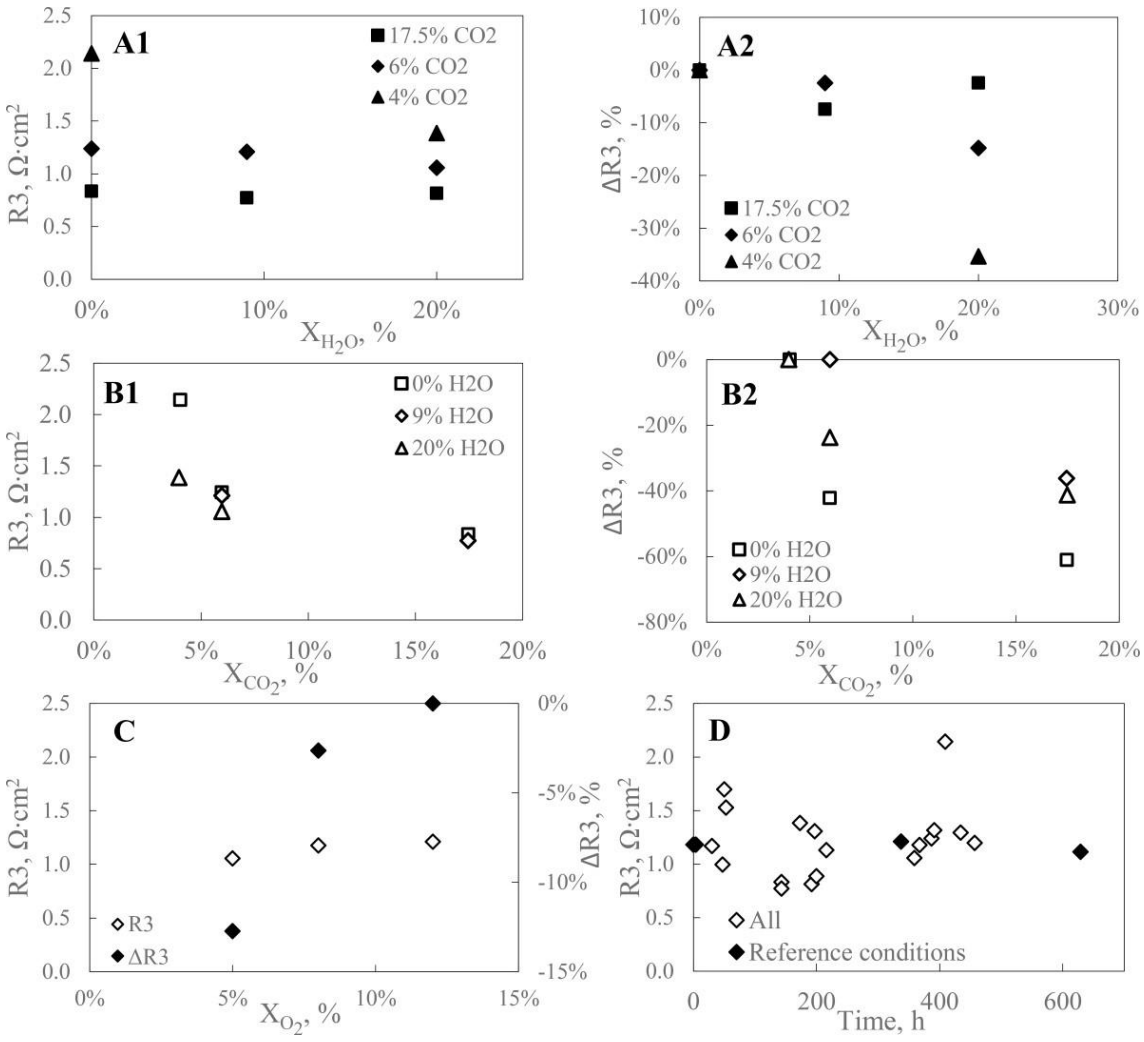

Figure 6. R3 dependence on the cathodic species content: water (A), carbon dioxide (B) and oxygen (C). R3 dependence on time (D) for the reference conditions (solid diamond) the whole test series (open diamonds).

Based on the presented data, it can be observed that:

- *R*3 strongly depends on the CO_2 fraction content; specifically, the lower the amount of CO_2 is and the higher is *R*3 (Figure 6, B1 and B2). This shows an expected resistance increase with the reduction of one of the main reagents in the cathodic reaction (1). The absence of H_2O blocks the access to the additional path of reactions (5) and (6), amplifying the mechanism.
- The dependence of *R*3 on water is not clear, but taking into account the values at very low CO_2 concentration, it is evident that the presence of H_2O allows a strong resistance reduction under this limiting operating condition (Figure 6, A1 and A2).

- *R3* seems to slightly increase with the O_2 concentration (Figure 6, C), but~~, when compared with the biggest variations due the CO_2 and H_2O, this behaviour results negligible~~ this results negligible when compared with the biggest variations due the CO_2 and H_2O. On the other hand, this light trend could be also due to a numerical balancing in the fitting procedure related to the strong decrease of in the Warburg impedance with the O_2 content increase (see Section 4.4), as evident in Figure 2, B.
- The experimental data collected in the studied range do not show a clear monotonic dependence of $R3$ on ageing (Figure 6, D).

The obtained results suggest that R3 is a suitable parameter to be monitored for the analysis of the effects of CO_2 composition on the MCFC performances, while ageing and O_2 effects are well described by the trend of parameter R1 and R2 respectively, as already discussed above.

4.4. Warburg R_W

In the range 1-1.5 Ohm·cm^2 the diffusion Warburg impedance prevails and arises as a third arc between the two main arcs when the H_2O concentration decreases (Figure 2, A). The water effect is negligible for high CO_2 concentration. O_2 has a similar behaviour (Figure 2, B). On the contrary, the Warburg impedance seems to be independent from the carbon dioxide fraction (Figure 2, D).

This feature confirms the mechanism already discussed which required the introduction of the Warburg impedance element in the equivalent circuit: the water effect appears as an additional oxide ion acceptor and, therefore, the increment of the water vapour partial pressure decreases the Warburg impedance coefficient, mainly at low CO_2 concentration.

As previously mentioned, Z_W is characterized by the coefficients R_W, Ψ and Φ, according to eq. (4).

Taking into account the obtained results, it can be observed that R_W, in good agreement with the previous considerations, varies with the H_2O content (Figure 7, A), decreasing for high amount of H_2O. A similar but significantly ~~more marked~~ remarkable trend is evident by increasing the O_2 content (Figure 7, C).

This large change dramatically affects the fitting procedure for high oxygen level and could compromise the correct determination of $R3$, coherently with the IV curves, so as mentioned in Section 4.3. In fact, R_W doubles its value when the O_2 fraction decreases from 12% to 5%. In this occurrence, the majority of the measured points, in the middle range of the frequency spectrum, belongs to the Warburg impedance. Specifically, the higher R_W is, the greater the influence of the Warburg impedance affecting the lower frequencies is. Consequently, few points are available to determine $R3$, giving rise to relevant effects on the fitting procedure. In addition, data available for $R3$ determination, in case of high R_W, belong to the lowest frequencies of the spectrum, with a wider distribution. This affects $R3$ accuracy, because low frequencies need long time of measurement during which the system exhibits fluctuations. Finally, as expected, R_W does not show any degrees of dependency on the CO_2 content in the mixture (Figure 7, B) nor on time/ageing (Figure 7, D). Therefore, it cannot be taken ~~in to~~ into account to measure the degradation of the cell performances.

Ψ and Φ depend on both physical parameters (L, the diffusion layer thickness, and D, the diffusivity coefficient) and adopted model (finite length of the diffusion layer). The experimental data show Ψ and Φ almost constant values and attest a negligible variation of D due to the cathodic composition (Figure 8, A, B and C). Moreover, this result confirms that the choice to operate at constant flow rate, involving constant fluid dynamics conditions, guarantees constant L in order to isolate the effect on the performance of only feeding composition. Regarding their dependence on cell degradation over ageing (Figure 8, D), Ψ and Φ vary in according to experimental fluctuation, without any dependence on H_2O, O_2 or CO_2 content.

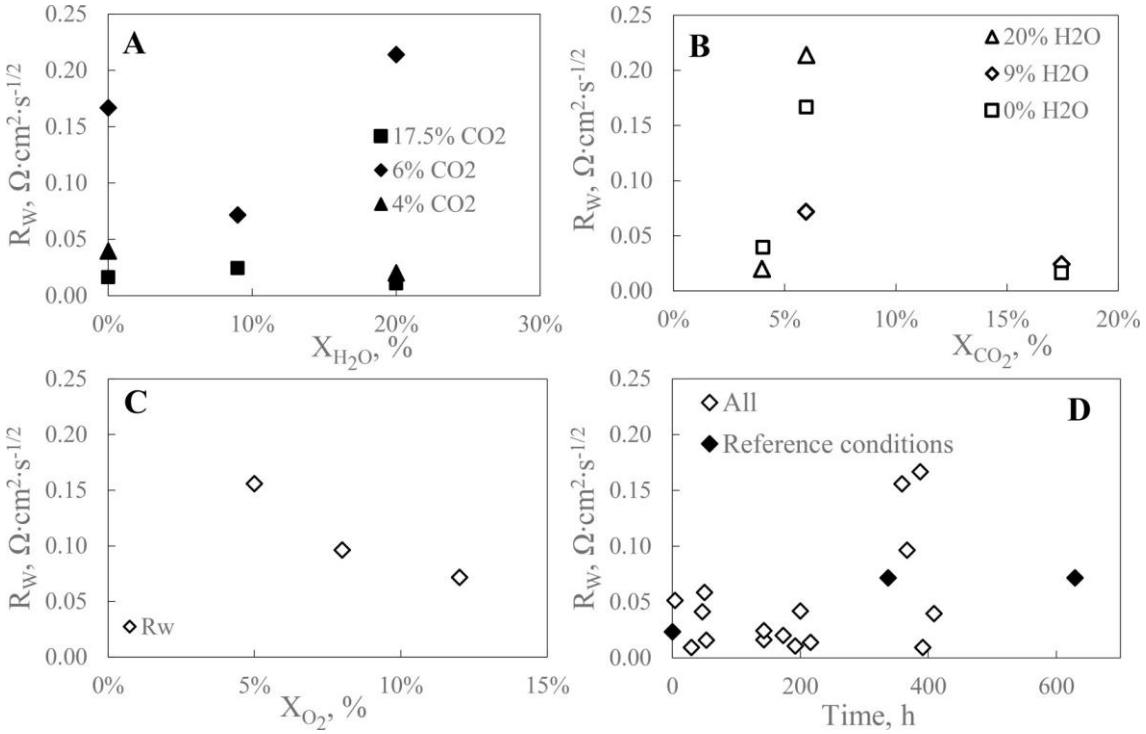

Figure 7. Warburg coefficient R_W dependence on the cathodic species content: water (A), carbon dioxide (B) and oxygen (C). R_W dependence on time (D) for the reference conditions (solid diamond) the whole test series (open diamonds).

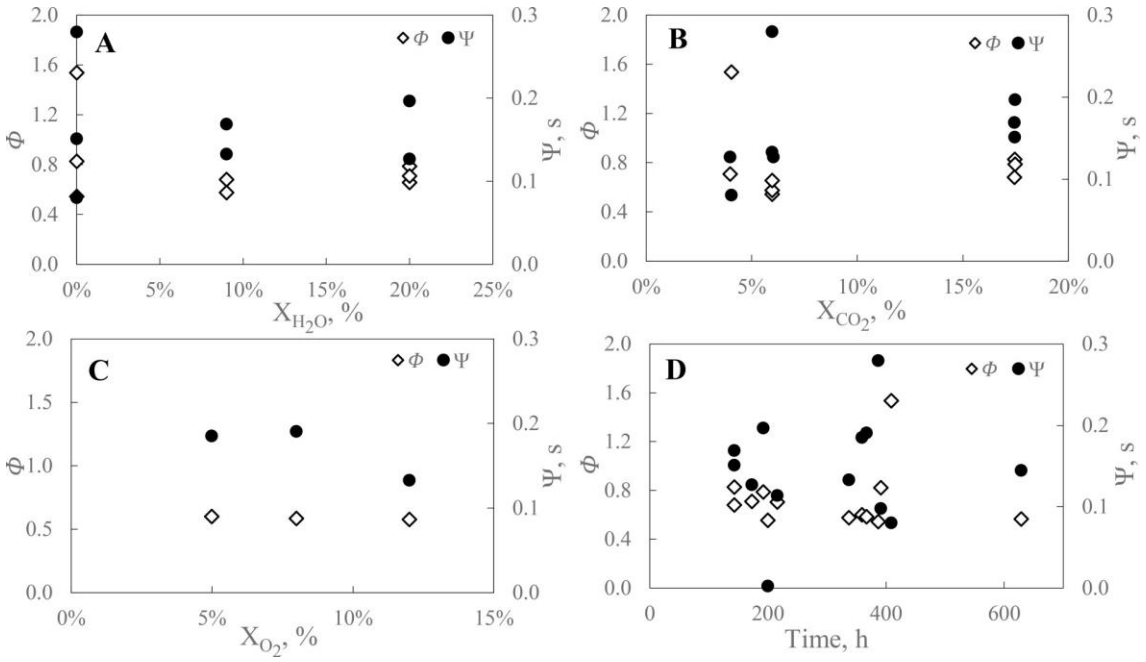

Figure 8. Warburg coefficient Φ and Ψ dependence on the cathodic species content: water (A), carbon dioxide (B) and oxygen (C). Φ and Ψ dependence on time (D) for the whole test series.

4.5. Comparison with kinetics model equation

The highlighted dependence of the equivalent circuit elements on the tested operating conditions suggests a comparison between these resistance elements and the contributions constituting the kinetics model presented by the authors in [49]:

$$R_{TOT} = R_{Ohm} + R_{CAT,O_2(CO_2)} + R_{CAT,cO_{2(H2O)}} + R_{AN,H_2}$$

$$= \mathrm{P}_1 \exp\left(\frac{\mathrm{P}_2}{T}\right) + \frac{\mathrm{P}_3 T \exp\left(\frac{\mathrm{P}_4}{T}\right)}{p \ln\left[1 - \frac{1.5}{1+\vartheta}\left(y_{CO_2} + \vartheta y_{H_2O}\right)\right]^{-1}} + \mathrm{P}_5 T \exp\left(\frac{\mathrm{P}_6}{T}\right) p^{-0.25} y_{O_2}^{-0.75} y_{CO_2}^{0.5} + \frac{\mathrm{P}_7 T \exp\left(\frac{\mathrm{P}_8}{T}\right)}{p \ln\left(1 + y_{H_2}\right)} \quad (8)$$

The model is a kinetic equation, expressed by eq. **(**8**)**, deduced through kinetic and thermodynamic theoretical considerations and with nine parameters (8 $\mathrm{P_i}$ and ϑ) experimentally identified.

~~Thanks to its implementation~~ Computationally implemented in the SIMF code [66] for the simulation of laboratory as well as industrial MCFCs, the model was validated by comparison with I-V curves showing a good fitting in a wide range of feeding compositions with an average error of 1% [20], [49].

The formulation proposes the total MCFC resistance written as a series of resistances:

1. R_{ohm}: a simplified expression of the internal resistance;
2. $R_{CAT,O_2(CO_2)}$: a cathode polarization resistance depending on the oxygen ions concentration expressed as a function of O_2 and CO_2 partial pressure according to the selected O_2 evolution path (in the above eq. **(**8**)** the superoxide one);
3. $R_{CAT,cO_{2(H2O)}}$: a cathode polarization resistance depending on the CO_2 partial pressure, where also the water contribution and the induced fluxes effects have been taken into account;
4. R_{AN,H_2}: an anode polarization resistance depending on the H_2 partial pressure, where also the induced fluxes effects have been considered.

It is evident a correspondence between these terms and the resistances previously discussed, so that R_{ohm} is equivalent to $R1$, $R_{CAT,O_2(CO_2)}$ has the same trend of $R2$ and $R_{CAT,cO_{2(H2O)}}$ corresponds to $R3$. R_{AN,H_2} in the tested cases is assumed constant and negligible.

This agreement results a mutual validation of the theoretical approach and of the empirical one proposed in this paper.

5. Conclusions

A systematic experimental campaign has led to verify the impact of variable cathodic conditions on the IV curve and impedance spectrum of an MCFC operating in typical CCS or CCU applications conditions. In particular, different contents in the cathodic feeding are considered not only of reactants (O_2 and CO_2), but also of water steam.

The monitoring of the degradation of the fuel cell is taken into account during the whole test campaign, to isolate the impact of the conditions that characterize the cathode, since time effects on MCFC performance are not negligible.

The MCFC behaviour is described through a parametric system by using the equivalent circuit method. A series of a resistance, a standard Randles-Ershler mesh and a modified Randles-Ersher mesh, with an extra Warburg impedance, compose the best equivalent circuit. The resistances (internal $R1$, polarization $R2$ and $R3$, and the Warburg R_W) are elicited by measurements/fitting.

The internal resistance $R1$ is mainly function of the ageing, therefore it is the natural candidate to monitor the MCFC degradation progress. The resistance $R2$ shows a clear dependency on O_2 reaction, while the resistance $R3$ should be considered as a promising parameter to monitor the MCFC behaviour as function of the cathodic feeding in terms of CO_2 and H_2O fractions.

A correspondence is put in evidence between these resistances and the ones constituting the kinetics model deduced by the authors on the basis of theoretical considerations and discussed in [49].

Consequently, a monitoring approach can be proposed where, according to the current specific operating conditions, performances of a complete cell can be evaluated through the analysis of the single parameter elicited by the EIS spectra. For example, the analysis of the $R1$ behaviour can be recommended to highlight possible ageing degradation at fixed cathodic mixture, while the analysis of $R2$ and $R3$ trend is of interest in case of working under variable cathodic mixture.

The present paper constitutes a basis for ~~next works~~ applications aimed to the development of a dedicated diagnostic tool in order to assess methodologies of real-time performance monitoring during the useful life of MCFCs in CCS, CCU as well as other industrial applications.

Acknowledgments

The authors wish to thank Dr. Cristina Moliner for her precious help in the revision work of the paper.

Bibliography

This aspect has been deeply discussed by the authors in the parallel modelling work [49] and is object of experimental validation in the following sections of the present paper.

[1] A. Mehmeti, F. Santoni, M. Della Pietra, and S. J. McPhail, "Life cycle assessment of molten carbonate fuel cells: State of the art and strategies for the future," *J. Power Sources*, vol. 308, pp. 97–108, Mar. 2016.

[2] G. Falcucci, E. Jannelli, M. Minutillo, S. Ubertini, J. Han, S. P. Yoon, and S. W. Nam, "Integrated numerical and experimental study of a MCFC-plasma gasifier energy system," *Appl. Energy*, vol. 97, pp. 734–742, 2012.

[3] J. Wee, "Molten carbonate fuel cell and gas turbine hybrid systems as distributed energy resources," *Appl. Energy*, vol. 88, no. 12, pp. 4252–4263, Dec. 2011.

[4] J. Milewski, M. Wołowicz, A. Miller, and R. Bernat, "A reduced order model of Molten Carbonate Fuel Cell: A proposal," *Int. J. Hydrogen Energy*, vol. 38, no. 26, pp. 11565–11575, Aug. 2013.

[5] L. Barelli, G. Bidini, S. Campanari, G. Discepoli, and M. Spinelli, "Performance assessment of natural gas and biogas fueled molten carbonate fuel cells in carbon capture configuration," *J. Power Sources*, vol. 320, pp. 332–342, Jul. 2016.

[6] S. Campanari, "Carbon dioxide separation from high temperature fuel cell power plants," *J. Power Sources*, vol. 112, no. 1, pp. 273–289, Oct. 2002.

[7] L. Caprile, B. Passalacqua, and a. Torazza, “Carbon capture: Energy wasting technologies or the MCFCs challenge?,” *Int. J. Hydrogen Energy*, vol. 36, no. 16, pp. 10269–10277, Aug. 2011.

[8] K. Sugiura, K. Takei, K. Tanimoto, and Y. Miyazaki, “The carbon dioxide concentrator by using MCFC,” *J. Power Sources*, vol. 118, no. 1–2, pp. 218–227, May 2003.

[9] J. Milewski, W. Bujalski, M. Wołowicz, K. Futyma, J. Kucowski, and R. Bernat, “Experimental investigation of CO2 separation from lignite flue gases by 100 cm2 single Molten Carbonate Fuel Cell,” *Int. J. Hydrogen Energy*, vol. 39, no. 3, pp. 1558–1563, Jan. 2014.

[10] G. Discepoli, G. Cinti, U. Desideri, D. Penchini, and S. Proietti, “Carbon capture with molten carbonate fuel cells: Experimental tests and fuel cell performance assessment,” *Int. J. Greenh. Gas Control*, vol. 9, pp. 372–384, Jul. 2012.

[11] I. Rexed, M. Della Pietra, S. J. McPhail, G. Lindbergh, and C. Lagergren, “Molten carbonate fuel cells for CO2 separation and segregation by retrofitting existing plants – An analysis of feasible operating windows and first experimental findings,” *Int. J. Greenh. Gas Control*, vol. 35, pp. 120–130, Apr. 2015.

[12] D. Sánchez, B. Monje, R. Chacartegui, and S. Campanari, “Potential of molten carbonate fuel cells to enhance the performance of CHP plants in sewage treatment facilities,” *Int. J. Hydrogen Energy*, vol. 38, no. 1, pp. 394–405, Jan. 2013.

[13] J. Milewski and J. Lewandowski, “Separating CO2 from Flue Gases Using a Molten Carbonate Fuel Cell,” *IERI Procedia*, vol. 1, no. 48, pp. 232–237, Jan. 2012.

[14] A. Amorelli, M. B. Wilkinson, P. Bedont, P. Capobianco, B. Marcenaro, F. Parodi, and A. Torazza, “An experimental investigation into the use of molten carbonate fuel cells to capture CO2 from gas turbine exhaust gases,” *Energy*, vol. 29, no. 9–10, pp. 1279–1284, Jul. 2004.

[15] U. Desideri, S. Proietti, P. Sdringola, G. Cinti, and F. Curbis, “MCFC-based CO2 capture system for small scale CHP plants,” *Int. J. Hydrogen Energy*, vol. 37, no. 24, pp. 19295–19303, Dec. 2012.

[16] M. Spinelli, M. C. Romano, S. Consonni, S. Campanari, M. Marchi, and G. Cinti, “Application of Molten Carbonate Fuel Cells in Cement Plants for CO2 Capture and Clean Power Generation,” *Energy Procedia*, vol. 63, pp. 6517–6526, 2014.

[17] S. Campanari, P. Chiesa, G. Manzolini, and S. Bedogni, “Economic analysis of CO2 capture from natural gas combined cycles using Molten Carbonate Fuel Cells,” *Appl. Energy*, vol. 130, pp. 562–573, Oct. 2014.

[18] S. Campanari, G. Manzolini, and P. Chiesa, “Using MCFC for high efficiency CO2 capture from natural gas combined cycles: Comparison of internal and external reforming,” *Appl. Energy*, vol. 112, pp. 772–783, Dec. 2013.

[19] U. Desideri, S. Proietti, G. Cinti, P. Sdringola, and C. Rossi, “Analysis of pollutant emissions from cogeneration and district heating systems aimed to a feasibility study of MCFC technology for carbon dioxide separation as retrofitting of existing plants,” *Int. J. Greenh. Gas Control*, vol. 5, no. 6, pp. 1663–

1673, Nov. 2011.

[20] E. Audasso, B. Bosio, and S. Nam, “Extension of an effective MCFC kinetic model to a wider range of operating conditions,” *Int. J. Hydrogen Energy*, vol. 41, no. 12, pp. 5571–5581, Apr. 2016.

[21] P. Greppi, B. Bosio, and E. Arato, “Membranes and Molten Carbonate Fuel Cells to Capture CO 2 and Increase Energy Production in Natural Gas Power Plants,” *Ind. Eng. Chem. Res.*, vol. 52, no. 26, pp. 8755–8764, 2013.

[22] E. Sisani, G. Cinti, G. Discepoli, D. Penchini, U. Desideri, and F. Marmottini, “Adsorptive removal of H2S in biogas conditions for high temperature fuel cell systems,” *Int. J. Hydrogen Energy*, vol. 39, no. 36, pp. 21753–21766, Dec. 2014.

[23] N. Di Giulio, E. Audasso, B. Bosio, J. Han, and S. J. McPhail, “Experimental influence of operating variables on the performances of MCFCs under SO2 poisoning,” *Int. J. Hydrogen Energy*, vol. 40, no. 19, pp. 6430–6439, 2015.

[24] N. Di Giulio, B. Bosio, V. Cigolotti, and S. W. Nam, “Experimental and theoretical analysis of H2S effects on MCFCs,” *Int. J. Hydrogen Energy*, vol. 37, no. 24, pp. 19329–19336, Dec. 2012.

[25] J.-E. Kim, J. Han, S. P. Yoon, S. W. Nam, T.-H. Lim, and H. Kim, “Mechanical properties of the lithium aluminate matrix for MCFC reinforced with metal oxide materials,” *Curr. Appl. Phys.*, vol. 10, no. 2, pp. S73–S76, Mar. 2010.

[26] E. Antolini, “The stability of molten carbonate fuel cell electrodes: A review of recent improvements,” *Appl. Energy*, vol. 88, no. 12, pp. 4274–4293, Dec. 2011.

[27] A. Buonomano, F. Calise, G. Ferruzzi, and A. Palombo, “Molten carbonate fuel cell: An experimental analysis of a 1kW system fed by landfill gas,” *Appl. Energy*, vol. 140, pp. 146–160, Feb. 2015.

[28] G. Discepoli, J. Milewski, and U. Desideri, “Off-design operation of coal power plant integrated with natural gas fueled molten carbonate fuel cell as CO2 reducer,” *Int. J. Hydrogen Energy*, pp. 1–11, Feb. 2016.

[29] EPA, “Draft Inventory of U.S. Greenhouse Gas Emissions and Sinks: 1990-2014,” 2016.

[30] J. R. Selman and Y. P. Lin, “Application of ac impedance in fuel cell research and development,” *Electrochim. Acta*, vol. 38, no. 14, pp. 2063–2073, Oct. 1993.

[31] T. Nishina, M. Takahashi, and I. Uchida, “Gas Electrode Reactions in Molten Carbonate Media IV. Electrode Kinetics and Mechanism of Hydrogen Oxidation in (Li + K)C03 Eutectic,” *J. Electrochem. Soc.*, vol. 137, no. 4, pp. 1112–1121, 1990.

[32] C. Boigues Muñoz, D. Pumiglia, S. J. McPhail, D. Montinaro, G. Comodi, G. Santori, M. Carlini, and F. Polonara, “More accurate macro-models of solid oxide fuel cells through electrochemical and microstructural parameter estimation – Part I: Experimentation,” *J. Power Sources*, vol. 294, pp. 658–668, Oct. 2015.

[33] C. Boigues Muñoz, D. Pumiglia, S. J. McPhail, G. Santori, D. Montinaro, G. Comodi, M. Carlini, and F.

Polonara, “More accurate macro-models of solid oxide fuel cells through electrochemical and microstructural parameter estimation – Part II: Parameter estimation,” *J. Power Sources*, vol. 286, pp. 321–329, Jul. 2015.

[34] H. Colón-Mercado, P. Ganesan, and B. Popov, “Performance studies of bare and Co-plated titanium alloy as cathode current collector in Molten Carbonate Fuel Cell (MCFC),” *Surf. Coatings Technol.*, vol. 201, no. 14, pp. 6452–6459, Apr. 2007.

[35] B. Huang, X. Ye, S. Wang, Q. Yu, H. Nie, Q. Hu, J. Shi, K. Hu, and T. Wen, “Electrochemical performance of Y2O3/NiO cathode in the molten Li0.62/K0.38 carbonates eutectics,” *Mater. Res. Bull.*, vol. 41, no. 10, pp. 1935–1948, Oct. 2006.

[36] M. J. Escudero, A. Ringuedé, M. Cassir, T. González-Ayuso, and L. Daza, “Porous nickel MCFC cathode coated by potentiostatically deposited cobalt oxide,” *J. Power Sources*, vol. 171, no. 2, pp. 261–267, Sep. 2007.

[37] L. Hu, I. Rexed, G. Lindbergh, and C. Lagergren, “Electrochemical performance of reversible molten carbonate fuel cells,” *Int. J. Hydrogen Energy*, vol. 39, no. 23, pp. 12323–12329, Aug. 2014.

[38] I. Rexed, C. Lagergren, and G. Lindbergh, “Effect of sulfur contaminants on MCFC performance,” *Int. J. Hydrogen Energy*, vol. 39, no. 23, pp. 12242–12250, Aug. 2014.

[39] H. Devianto, E. Simonetti, S. J. McPhail, F. Zaza, V. Cigolotti, C. Paoletti, A. Moreno, A. La Barbera, and I. Luisetto, “Electrochemical impedance study of the poisoning behaviour of Ni-based anodes at low concentrations of H2S in an MCFC,” *Int. J. Hydrogen Energy*, pp. 1–7, Apr. 2012.

[40] X. YUAN, H. WANG, J. COLINSUN, and J. ZHANG, “AC impedance technique in PEM fuel cell diagnosis—A review,” *Int. J. Hydrogen Energy*, vol. 32, no. 17, pp. 4365–4380, Dec. 2007.

[41] P. Piela, R. Fields, and P. Zelenay, “Electrochemical Impedance Spectroscopy for Direct Methanol Fuel Cell Diagnostics,” *J. Electrochem. Soc.*, vol. 153, no. 10, p. A1902, 2006.

[42] J. I. Gazzarri and O. Kesler, “Electrochemical AC impedance model of a solid oxide fuel cell and its application to diagnosis of multiple degradation modes,” *J. Power Sources*, vol. 167, no. 1, pp. 100–110, May 2007.

[43] J. I. Gazzarri and O. Kesler, “Non-destructive delamination detection in solid oxide fuel cells,” *J. Power Sources*, vol. 167, no. 2, pp. 430–441, May 2007.

[44] L. Barelli, E. Barluzzi, and G. Bidini, “Diagnosis methodology and technique for solid oxide fuel cells: A review,” *Int. J. Hydrogen Energy*, vol. 38, no. 12, pp. 5060–5074, Apr. 2013.

[45] G. L. Lee and J. R. Selman, “ac-superimposed-on-dc characteristics of fuel cell electrode reactions—part I. Partially submerged smooth electrode,” *Electrochim. Acta*, vol. 38, no. 15, pp. 2281–2290, Oct. 1993.

[46] M. Della Pietra, G. Discepoli, B. Bosio, S. J. McPhail, L. Barelli, G. Bidini, and A. Ribes-Greus, “Experimental investigation of SO2 poisoning in a Molten Carbonate Fuel Cell operating in CCS configuration,” *Int. J. Hydrogen Energy*, pp. 1–15, Jun. 2016.

[47] C.-G. Lee, K.-S. Ahn, H.-C. Lim, and J.-M. Oh, “Effect of carbon monoxide addition to the anode of a molten carbonate fuel cell,” *J. Power Sources*, vol. 125, no. 2, pp. 166–171, Jan. 2004.

[48] J. Milewski, G. Discepoli, and U. Desideri, “Modeling the performance of MCFC for various fuel and oxidant compositions,” *Int. J. Hydrogen Energy*, vol. 39, no. 22, pp. 11713–11721, Jul. 2014.

[49] E. Arato, E. Audasso, L. Barelli, B. Bosio, and G. Discepoli, “Kinetic modelling of molten carbonate fuel cells: Effects of cathode water and electrode materials,” *J. Power Sources*, vol. 330, pp. 18–27, Oct. 2016.

[50] P. M. Gomadam and J. W. Weidner, “Analysis of electrochemical impedance spectroscopy in proton exchange membrane fuel cells,” *Int. J. Energy Res.*, vol. 29, no. 12, pp. 1133–1151, 2005.

[51] F. Migliardini and P. Corbo, “CV and EIS study of hydrogen fuel cell durability in automotive applications,” *Int. J. Electrochem. Sci.*, vol. 8, no. 9, pp. 11033–11047, 2013.

[52] X. Yan, M. Hou, L. Sun, D. Liang, Q. Shen, H. Xu, P. Ming, and B. Yi, “AC impedance characteristics of a 2 kW PEM fuel cell stack under different operating conditions and load changes,” *Int. J. Hydrogen Energy*, vol. 32, no. 17, pp. 4358–4364, 2007.

[53] S. Campanari, P. Chiesa, G. Manzolini, A. Giannotti, F. Federici, P. Bedont, and F. Parodi, “Application of MCFCs for active CO2 capture within natural gas combined cycles,” *Energy Procedia*, vol. 4, pp. 1235–1242, Jan. 2011.

[54] V. Hoenig, H. Hoppe, K. Koring, and J. Lemke, “ECRA CCS Project - Report about Phase II,” Duesseldorf, 2009.

[55] J.-H. Koh, B. S. Kang, and H. C. Lim, “Effect of various stack parameters on temperature rise in molten carbonate fuel cell stack operation,” *J. Power Sources*, vol. 91, no. 2, pp. 161–171, Dec. 2000.

[56] H. Morita, M. Komoda, Y. Mugikura, Y. Izaki, T. Watanabe, Y. Masuda, and T. Matsuyama, “Performance analysis of molten carbonate fuel cell using a Li/Na electrolyte,” *J. Power Sources*, vol. 112, no. 2, pp. 509–518, Nov. 2002.

[57] T. Nishina, S. Ohuchi, K. Yamada, and I. Uchida, “Water effect on oxygen reduction in molten (Li + K)CO3 eutectic,” *J. Electroanal. Chem.*, vol. 408, no. 1–2, pp. 181–187, May 1996.

[58] K. Hemmes and J. R. Selman, “O 2 -reduction at high temperature: MCFC,” in *Handbook of Fuel Cells*, vol. 2, W. Vielstich, A. Lamm, and A. H. Gasteiger, Eds. Chichester, UK: John Wiley & Sons, Ltd, 2010, pp. 570–586.

[59] B. B. Davé, R. E. White, S. Srinivasan, and A. J. Appleby, “Impedance Analysis for Oxygen Reduction in a Lithium Carbonate Melt: Effects of Partial Pressure of Carbon Dioxide and Temperature,” *J. Electrochem. Soc.*, vol. 140, no. 8, p. 2139, 1993.

[60] J.-B. Jorcin, M. E. Orazem, N. Pébère, and B. Tribollet, “CPE analysis by local electrochemical impedance spectroscopy,” *Electrochim. Acta*, vol. 51, no. 8–9, pp. 1473–1479, Jan. 2006.

[61] C. L. Alexander, B. Tribollet, and M. E. Orazem, “Contribution of Surface Distributions to Constant-

Phase-Element (CPE) Behavior: 1. Influence of Roughness," *Electrochim. Acta*, vol. 173, pp. 416–424, Aug. 2015.

[62] T. Nishina, I. Uchida, and J. R. Selman, "Gas Electrode Reactions in Molten Carbonate Media Part V. Electrochemical Analysis of th.e Oxygen Reduction Mechanism at a Fully Immersed Gold Electrode," *J. Electrochem. Soc.*, vol. 141, no. 5, p. 1191, 1994.

[63] P. Tomczyk and M. Mosiałek, "Investigation of the oxygen electrode reaction in basic molten carbonates using electrochemical impedance spectroscopy," *Electrochim. Acta*, vol. 46, no. 19, pp. 3023–3032, Jun. 2001.

[64] D. R. Franceschetti, J. R. MacDonald, and R. P. Buck, "Interpretation of Finite-Length-Warburg-Type Impedances in Supported and Unsupported Electrochemical Cells with Kinetically Reversible Electrodes," *J. Electrochem. Soc.*, vol. 138, no. 5, p. 1368, 1991.

[65] C.-Y. Yuh and J. R. Selman, "The Polarization of Molten Carbonate Fuel Cell Electrodes," *J. Electrochem. Soc.*, vol. 138, no. 12, pp. 3649–3656, 1991.

[66] B. Bosio, D. Marra, and E. Arato, "Thermal management of the molten carbonate fuel cell plane," *J. Power Sources*, vol. 195, no. 15, pp. 4826–4834, Aug. 2010.